

Article

Not peer-reviewed version

Adhesive Single-Lap Joints Evaluation Using Ultrasonic Guided Waves

[Mário Santos](#) * and [Jaime Batista Santos](#)

Posted Date: 9 May 2023

doi: 10.20944/preprints202305.0557.v1

Keywords: guided waves; ultrasounds; adhesive lap joints; simulation



Preprints.org is a free multidiscipline platform providing preprint service that is dedicated to making early versions of research outputs permanently available and citable. Preprints posted at Preprints.org appear in Web of Science, Crossref, Google Scholar, Scilit, Europe PMC.

Copyright: This is an open access article distributed under the Creative Commons Attribution License which permits unrestricted use, distribution, and reproduction in any medium, provided the original work is properly cited.

Article

Adhesive Single-Lap Joints Evaluation Using Ultrasonic Guided Waves

Mário Santos * and Jaime Santos

University of Coimbra, CEMMPRE, ARISE, Department of Electrical and Computer Engineering, 3030-290 Coimbra, Portugal

* Correspondence: marioj@deec.uc.pt; Tel.: +351-239-796200

Abstract: This work deals with the evaluation of adhesive single-lap joints using ultrasonic guided waves. An adhesive bonded lap joint can be modelled as a three-layer system made up of two adherents and an adhesive. The propagation of guided waves in the joint is developed from matrix formulations. The behavior of the different guided wave modes that propagate in the bonded region is characterized and it is found that their relative amplitudes can be estimated based on the properties of the incoming wave that propagates in the non-bonded region. It was verified that the excitation of these modes is ruled by the degree in which the shapes of both modes match each other. A 3D simulation of two aluminium bonded plates using 500 kHz ultrasonic transducers in a pitch and catch configuration was implemented using the Matlab k-Wave toolbox. Scattering effects due to some produced defects located in the bond line of the lap joints were simulated. Experimental setup with some artificial defects produced in the aluminum joints were used in order to compare with the simulated. Qualitative agreement was observed for the two approaches. The observed deviation can be due to the different characteristics of the experimental and simulated defects.

Keywords: guided waves; ultrasounds; adhesive lap joints; simulation

1. Introduction

Adhesively bonded joints have been used with great success in several fabrication processes, because they promote a more even stress distribution, when compared to other conventional joints, such as bolting, riveting and spot welding, where high stress concentrations can occur. The possibility of obtaining lighter and waterproof structures with reduced corrosion risks contributes greatly for the adhesive joints use, working as an alternative to the conventional joints in several industries, including aerospace, automotive, and energy.

The fabrication of adhesive bond joints can originate defects of three different types: adhesive defects that are related to the weak bonding between the adhesive and the adherend, cohesive defects related to the mechanical properties of the adhesive, and gross defects, such as cracking, disbonding, porosity, and voids, [1]. The formation of voids or absence of adhesive in the bond line is a great concern in industry [2], so such defects will be studied and characterized in this work.

The development of non-destructive methods is essential for the condition monitoring of bonded structures. Probably, one of the most used methods is based on ultrasound guided waves. When compared to conventional point by point method, the guided waves are more attractive, because once generated they propagate over considerable distances with low attenuation, which allows inspecting large parts with considerable time saving.

Guided waves have often been used for defect detection in structures like strips, plates, or pipes [3–10]. They have also proved to be effective for inspecting adhesive joints [11–15] and adhesive bonds between composites [16,17], and for the adhesion level evaluation [18]. Several studies using the ultrasound guided waves to assess the bonding quality of metal/epoxy/metal joints can be found in the literature, such as, comparison between air coupling and immersion techniques [19], analysis of the spectra of the lowest-order antisymmetric (A_0) Lamb wave mode for tangential bond stiffness

evaluation [20], defects detection in the adhesive films and evaluation of their geometry by means of a weighted root mean square damage imaging algorithm [21,22], evaluation of interference effects of elastic waves generated by piezo sensors, excited with tone bursts of different extensions, with the length of the disbond [23], study of the non-linear Lamb wave behavior [24,25], and development of a finite difference model to simulate and validate experiments using PZTs in bonded aluminium plates [26].

Simulation allows predicting the ultrasound wave propagation in a particular medium and can be used to prove analytical and experimental approaches. Currently, the improvement of computational resources makes the implementation of numerical or grid-based methods possible. Recent works have used finite element methods (FEM) to accurately mimic wave propagation through bonded lap joints [19,23,26–29]. One of the major drawbacks of elastic wave models based on low-order finite difference or finite element schemes is the large number of grid points per wavelength required to avoid numerical dispersion. As an alternative, the k-Wave, which is an available third-party MATLAB toolbox, makes use of a Fourier domain pseudo spectral method for faster simulation and reconstruction of photoacoustic wave fields in a way that uses less memory and is user-friendly [30,31]. Many authors have used the k-Wave toolbox in diverse NDT applications related to nonlinear ultrasound propagation in absorbing media [32], attenuation in ultrasonic computed tomography [33], time domain power law attenuation in breast and liver tissues [34], one-sided ultrasonic nondestructive evaluation [35], high intensity focused ultrasound [36], ultrasonic transducer field modelling [37], 3-D ultrasound imaging [38], A-scan ultrasound simulation in ophthalmology [39], microflaw detection in carbon fiber reinforced polymers [40], and guided waves in layered structures [41,42].

In the present study, the authors intend to implement a 3D simulation model of two aluminium plates bonded by an epoxy adhesive layer, using the k-Wave tool. Simulated defects with different sizes are introduced in the adhesive layer. A pitch and catch experimental setup is also used to detect and characterize the same type of defects. Simulated results are then compared with the experimental ones.

2. Theory

2.1. Ultrasound Guided Waves Propagation in a Single Plate

Lamb waves are a type of guided ultrasonic waves that exist in plate structures placed in vacuum, which can propagate relatively long distances. They are very useful to detect disbonds, corrosion and delaminations, efficiently [43–46]. If plates are immersed in water these waves are called leaky Lamb waves, due to the energy leakage into the surrounding fluid. The well-known dispersion equations that govern symmetrical (Eq.1) and antisymmetrical (Eq.2) leaky Lamb wave modes were introduced by Viktorov [43],

$$\frac{\tan(qh)}{\tan(ph)} + \frac{4k^2pq}{(q^2-k^2)^2} - i \frac{\rho_0 k_T^4 p \tan(qh)}{\rho \sqrt{k_0^2 - k^2} (q^2 - k^2)^2} = 0, \quad (1)$$

$$\frac{\tan(ph)}{\tan(qh)} + \frac{4k^2pq}{(q^2-k^2)^2} + i \frac{\rho_0 k_T^4 p}{\rho \sqrt{k_0^2 - k^2} (q^2 - k^2)^2 \tan(qh)} = 0, \quad (2)$$

where i is the unit imaginary number, h is half the thickness of the plate, $p = \sqrt{k_L^2 - k^2}$, $q = \sqrt{k_T^2 - k^2}$, where $k_L = \frac{\omega}{c_L}$, $k_T = \frac{\omega}{c_T}$, $k = \frac{\omega}{c_p}$, $k_0 = \frac{\omega}{c_0}$, ω is the angular frequency, c_L is the longitudinal velocity in the plate, c_T the transversal velocity in the plate, c_p is the phase velocity of a certain propagation mode and c_0 is the velocity in the surrounding fluid. The plate and fluid densities are ρ and ρ_0 , respectively.

The transcendental Eqs. (1) and (2) give rise to an infinite number of solutions that correspond to the propagation modes. The imaginary part of each equation represents the fluid influence. If this is not present, the equations characterize the plate in vacuum. The leakage to the fluid is responsible for attenuation, which is strongly dependent on the ratio of in-plane and out-of-plane displacements

at the plate surfaces, for a given mode. For a particular propagation mode the phase velocity is complex, $c_p = c_{pr} + ic_{pi}$, which gives rise to a complex wavenumber, $k = \frac{\omega}{c_p} = \frac{\omega}{c_{pr} + ic_{pi}} = k_r + ik_i$ [47]. The real part k_r represents the propagation properties of the wave and k_i is related to leakage attenuation. Considering that usually $c_{pr} \gg c_{pi}$, then after some manipulation the complex wavenumber can be represented as,

$$k \cong \frac{\omega}{c_{pr}} - i \frac{\omega c_{pi}}{c_{pr}^2}. \quad (3)$$

The absolute value of the imaginary part of Eq. 3 represents an exponential decay, usually called attenuation coefficient, α (Np/m). The solutions of the dispersion equations for a plate in vacuum are very similar to the real part of the solutions for an immersed plate, because it has been shown that the surrounding fluid gives rise to very small variations in the wave velocity [48].

The particle displacement variation with plate thickness for each propagation mode is also very important. For the case of an immersed plate, if long range propagation is needed, then a low out-of-plane displacement must be assured to prevent the occurrence of great losses, due to leakage to the fluid. The displacements can be obtained using the method of potentials and the boundary conditions at plate surface. For a plate in vacuum oriented in X direction and with the thickness in Z direction, coincident with wave propagation direction, the in-plane (u_{xs}) and out-of-plane (u_{zs}) displacements of symmetric modes are given by [43,44]

$$u_{xs} = \frac{q^2 - k^2}{2p} \frac{\sin(qh)}{\sin(ph)} \cos(pz) - q \cos(qz), \quad (4)$$

$$u_{zs} = \frac{q^2 - k^2}{2k} \frac{\sin(qh)}{\sin(ph)} \sin(pz) + k \sin(qz), \quad (5)$$

and the displacements for the anti-symmetric modes (u_{xa}) and (u_{za}) by

$$u_{xa} = -\frac{q^2 - k^2}{2p} \frac{\cos(qh)}{\cos(ph)} \sin(pz) + q \sin(qz), \quad (6)$$

$$u_{za} = \frac{q^2 - k^2}{2k} \frac{\cos(qh)}{\cos(ph)} \cos(pz) + k \cos(qz). \quad (7)$$

For the case of a water immersed plate, equations (4) to (7) become complex, which can be interpreted physically as a small angle rotation of the ellipse displacement axes from the reference coordinate system [49]. Nevertheless, the real part of the displacements practically coincides with the displacements obtained from equations (4) to (7) [44]. So, as approximation, these equations can be used to represent the displacements as a function of plate thickness in immersion cases.

In analogy with optical phenomena, when an ultrasound wave reaches a boundary between two different media obliquely, refracted waves can occur with different transmission angles than the incident one. The incident (θ_1) and transmitted (θ_2) angles related to the normal plane are correlated by the well-known Snell's law, given by

$$C_1 \sin(\theta_2) = C_2 \sin(\theta_1), \quad (8)$$

where C_1 and C_2 are the propagation velocities in the different media. In practice, if one intends exciting a specific propagation mode in a plate, the phase velocity c_p (obtained from the dispersion curves) coincides with C_2 , and in this case $\theta_2 = 90^\circ$, since the propagation develops along the plate. Then, knowing the C_1 value, which corresponds to the propagation velocity in the fluid (c_0), the angle of incidence θ_1 can be easily obtained, to generate the desired propagation mode

$$\theta_1 = \arcsin\left(\frac{c_0}{c_p}\right). \quad (9)$$

Each Lamb wave mode is associated with an angle of re-emission, that by reciprocity is equal to the angle of incidence.

2.2. Propagation of Ultrasonic Guided Waves in Adhesively Bonded Joints

The ultrasound guided wave propagation in a bonded lap joint can be modeled as the propagation in a multilayer structure, composed of two adherents and one adhesive. The transfer matrix method is certainly the most important technique used to study this problem and find the complex phase velocity of each one propagation modes. First used by Haskell [50] for modelling propagation in seismology, the method was later adapted for studying the ultrasound guided wave propagation, by several researchers [51–55]. The method considers that there are four generic waves in each layer, such as, two longitudinal waves (L+, L-) and two transversal ones (T+, T-), where the sign (+) indicates upward direction, and (-) indicates downward direction. So, a field matrix (D) that describes the relationship between the displacements (u), stresses (σ) and wave amplitudes (A) at any location in a layer, can be established as

$$\begin{bmatrix} u_x \\ u_z \\ \sigma_x \\ \sigma_z \end{bmatrix} = [D] \begin{bmatrix} A_{L+} \\ A_{L-} \\ A_{T+} \\ A_{T-} \end{bmatrix} \quad (10)$$

In the process, the equations for the intermediate interfaces are eliminated, so that the fields in all layers of the structure are described only in terms of the external boundary conditions. The modal solutions can be obtained by solving the resulting matrix system and the so-called dispersion curves, which represent the allowed propagation guided modes in the structure as function of frequency. The behavior of these guided modes is like those obtained through Eq. (1) and (2). Details about the method are described elsewhere [56].

3. Materials and methods

3.1. Simulation model

The simulation functions in k-Wave require four input structures, namely the properties of the computational grid, representing the medium through which the acoustic waves propagate, the material properties of the medium, the properties and locations of acoustic sources, and the properties and locations of the sensor points used to collect the pressure and velocity fields over time. When the acoustic waves reach the edge of the computational domain, they are absorbed by a special type of anisotropic absorbing boundary layer known as a perfectly matched layer (PML). The schematic of the 3D simulation setup is presented in Figure 1 and its dimensions are: X=126 mm, Y=32 mm and Z=18 mm. The spatial resolution is 150 μ m. Each plate is 90 mm in length, 30 mm in width and 4 mm in thickness. The section of bonded region is of 60 mm x 30 mm. The adhesive thickness is 150 μ m. The emitter and receiver transducers are identical, with 25 mm in diameter. The incidence and reception angles are equal and given by Eq. (9). The defects were simulated by introducing air (absence of adhesive) with circular shape in the center of the joint region.

The acoustic properties of the materials used in the simulation are presented in Table 1. For water and air, the values were taken from literature [57]. For aluminium and epoxy the properties were obtained experimentally using a conventional pulse echo technique. For aluminium a 10 MHz transducer was used, due to the small thickness of the plates. As the thickness of the epoxy layer is very small, a cylinder with 20 mm height and 300 mm diameter was constructed to allow velocities' measurements. The densities were taken from manufacturer's specifications.

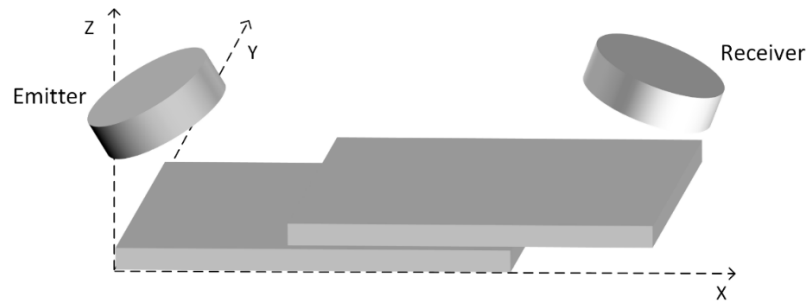


Figure 1. Schematic of the simulation setup for an adhesively bonded single lap joint inspection using pitch and catch configuration and guided waves.

Table 1. Acoustic properties of materials used in simulation.

Material	Density [Kg/m ³]	Longitudinal Velocity [m/s]	Transversal Velocity [m/s]
Water	1000	1500	-
Epoxy	1077	2540	1055
Aluminium	2660	6300	3130
Air	1.2	340	-

3.2. Experimental setup

The ultrasonic experimental setup illustrated in Figure 2 was used to evaluate the defects. It is composed by a Panametrics pulser/receiver model 5800, a pair of immersion broadband transducers (Imasonic model IM 0.5 25 P) with 500 kHz central frequency and 25 mm active diameter, and a Tektronix digital oscilloscope (model TDS1002B). The aluminium alloy (5083-O) plates are 200 mm in length, 125 mm in width and 4 mm in thickness. The size of bonded region is of 60 mm x 125 mm (whole width). The bonded zone has the same dimensions as the one presented in the simulation model described in the previous section.

The used plates were bonded together by means of an epoxy adhesive (Araldite 2014, Vantico, Duxford, Cambridge, UK), of 150 μm in thickness, achieved by a uniform pressure of 0.1 Kg/m². The adhesive was then cured according to the manufacturer's instructions at room temperature (25°C) for 24 h.

The used approach to produce artificial defects in the bonded line consisted of removing a circular portion of aluminium equal to the adhesive thickness in one of the plates, and then that zone is covered with sticky tape to avoid adhesive penetration, as described in [47].



Figure 2. Experimental setup.

4. Results

4.1. Phase velocities and displacements in a single plate in water

The solutions for the phase velocity were obtained from Eq. (1) and (2) using an iterative optimization algorithm. The first four propagation modes that correspond to the real part of the solutions for the aluminium plates used in this study, are shown in Figure 3. Figure 4 presents the leakage attenuation due to water, for the fundamental modes S0 and A0, obtained from the imaginary part of the equation (3). According to the used frequency (500kHz), it was selected the propagation mode S0, due to the high spatial separation compared to the other modes and the low attenuation compared to A0, allowing easier amplitude measurements.

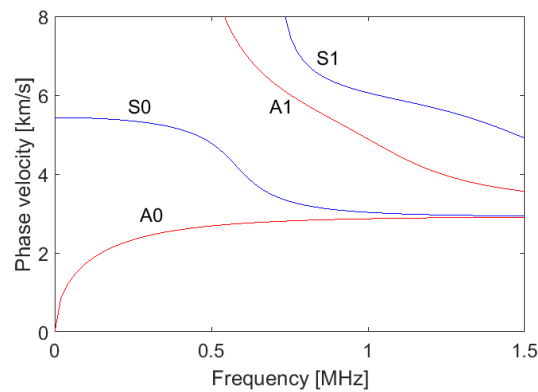


Figure 3. Phase velocity of the first four propagation guided modes for an aluminium plate with 4 mm in thickness immersed in water.

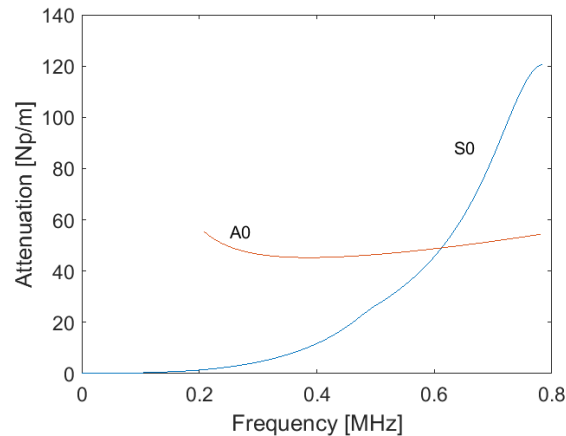


Figure 4. Leaky attenuation of the fundamental modes S0 and A0 in an aluminium plate with 4 mm in thickness immersed in water.

From Eq. (4) to (7), there were obtained the in-plane (u_x) and out-of-plane (u_z) displacements for S0 and A0, which are presented in Figure 5. The higher value of u_z for A0 mode, when compared to S0 mode, justify the high value of leakage attenuation observed in the Figure 4.

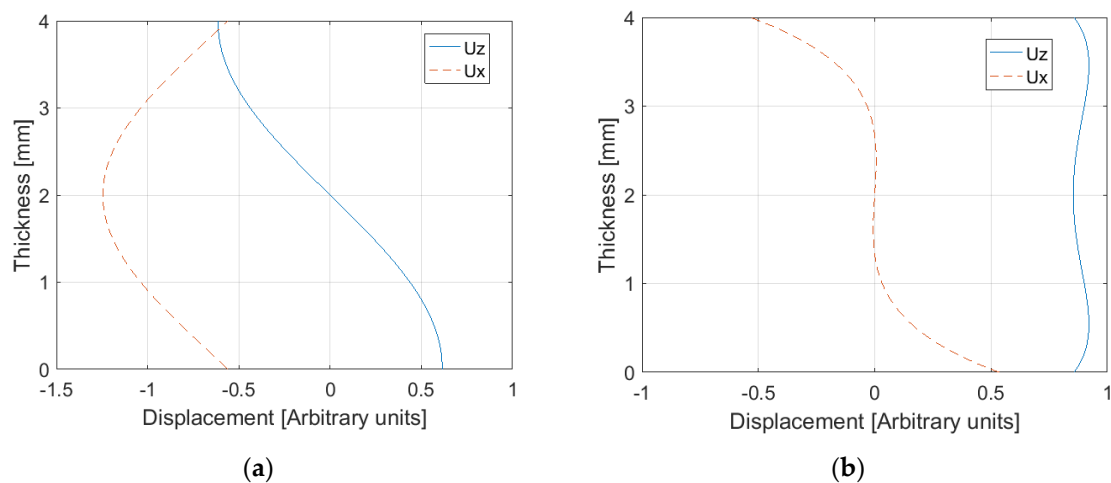


Figure 5. Displacements of the fundamental modes in an aluminium plate with 4 mm thickness: (a) S0; (b) A0.

4.2. Phase velocities and displacements in a bonded lap joint in water

For the bonded region the transfer matrix method introduced in the section 2.2 was used to obtain the modal solutions of the matrix system. The real part of the solutions, which is the phase velocity of the different modes, is presented in Figure 6.

The total thickness of the system is 8.15 mm (two 4 mm aluminium plates and 0.15 mm adhesive), so for the working frequency, four differences modes coexist: A0, S0, A1 and S1. The behavior is very similar to the previously obtained for the single plate, which is justified by the fact the system is mostly composed by aluminium with a very small amount of epoxy. The behavior difference characterizes by an increase of the number of propagation modes, which is related to the increase of the thickness. The attenuation values due to leakage for 500 kHz were obtained in the same way as previously for the single plate and are presented in Table 2.

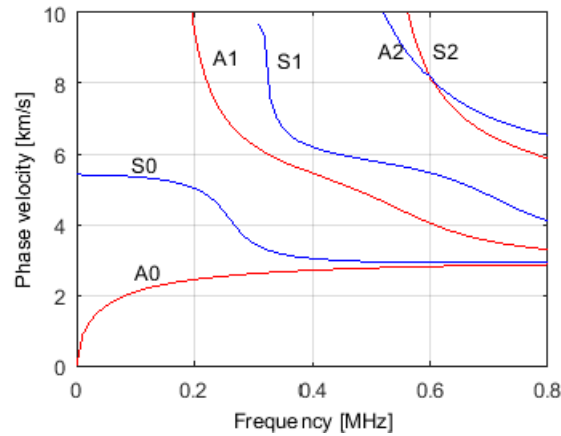
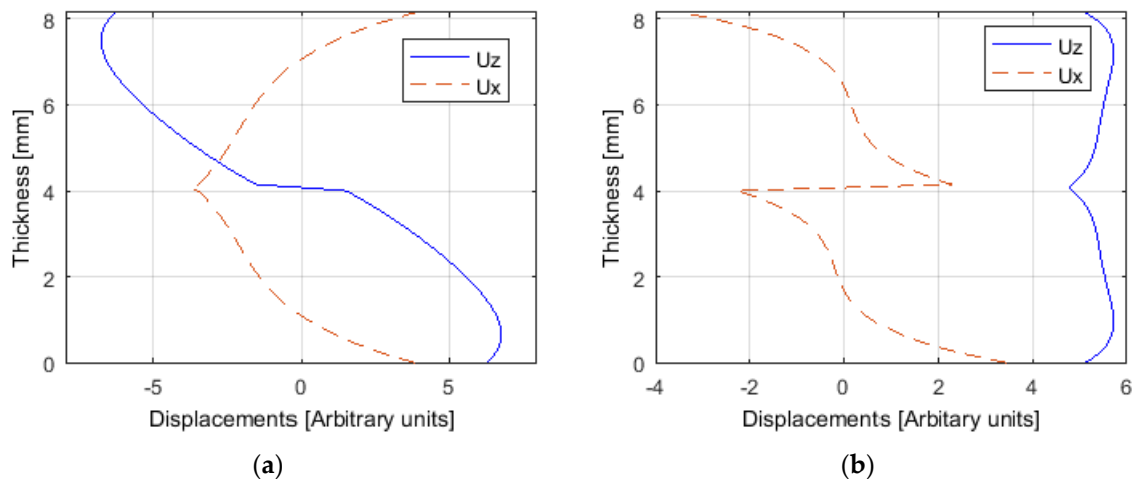


Figure 6. Phase velocity dispersion curves for two bonded aluminium plates immersed in water.

Table 2. Attenuation due to leakage to the fluid in the bonded plate region for the different propagation modes.

Mode	A0	S0	A1	S1
Attenuation [Np/m]	22.7	37.5	10.5	0.1

The displacements for the mentioned modes can be also obtained using the matrix method [56]. Considering the boundary conditions for all interfaces, it is obtained a matrix composed by the amplitude coefficients for the three layers. As the system is immersed, there are two additional unknowns corresponding to the amplitude of longitudinal waves at the water bottom boundary and at the top boundary water. By solving the matrix system, the displacement values in arbitrary units as a function of the thickness were evaluated and are presented in Figure 7. There is now a more complex pattern when compared with the single plate one, which is due to the epoxy adhesive layer. Looking at the displacements at the surface of the system, that are in contact with the water, the relation between the out-of-plane and in-plane values agrees with the attenuation values presented in Table 2. For example, for the S1 mode the displacement is essentially in-plane, giving rise to extremely low attenuation values. For the A1 mode, the two types of displacements are similar, giving rise to already noticeable attenuation values. Finally, for A0 and S0 modes, the out-of-plane displacements are greater than the in-plane ones, leading to higher attenuations.



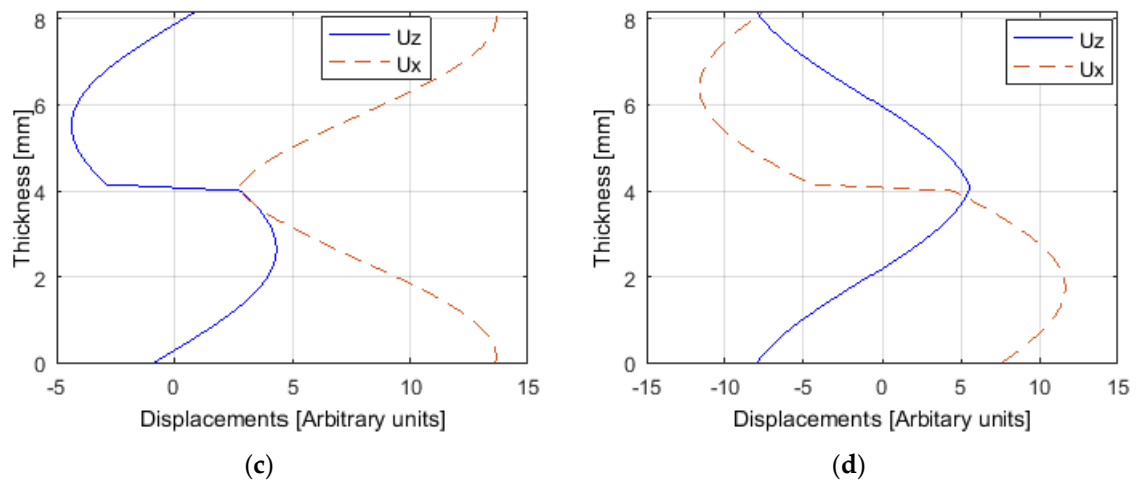


Figure 7. Displacements of the four existing modes in bonded region: (a) S0; (b) A0; (c) S1; (d) A1.

4.3. Guided waves propagation simulation

The k-Wave function used for the simulation is `psdElastic3D`, based on the pseudo spectral time domain (PSTD) method, which is able to simulate the time-domain propagation of elastic waves through a three-dimensional homogeneous or heterogeneous medium [58]. The simulation model presented in section 2.3 was implemented in a computer with an Intel® Core™ i7-4790 processor and 16GB RAM, with a Nvidia GeForce GTX1080 Ti GPU, 11.26 GB RAM. For the available hardware and the presented geometry, the maximum resolution (minimum grid point spacing) was limited to 150 μm . This resolution gave rise to 21.47x10⁶ voxels (840x213x120). The source was excited with a three-cycle burst, 500 kHz central frequency, as shown in Figure 8 (a). Figure 8 (b) illustrates the respective spectrum.

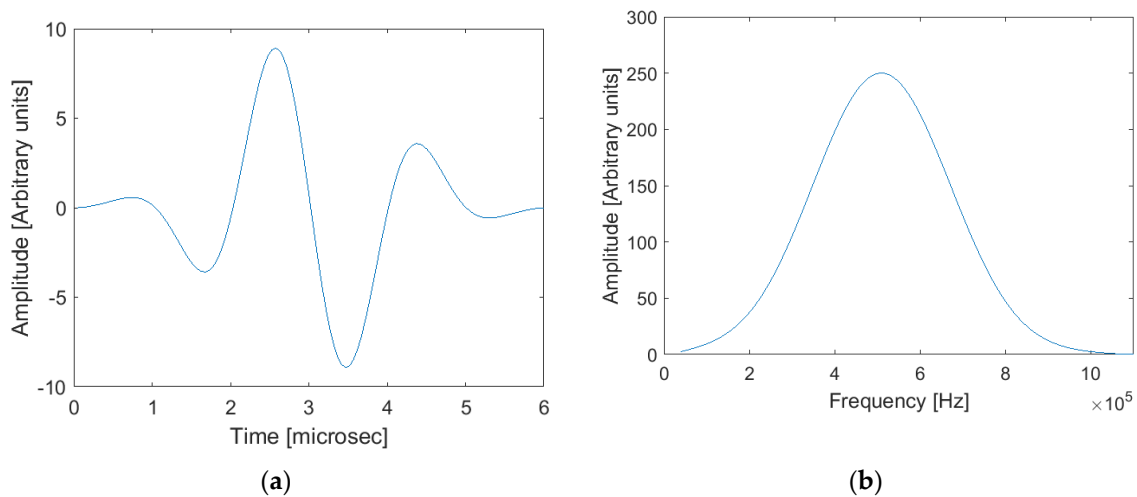


Figure 8. Excitation signal: (a) time domain; (b) frequency domain.

For model validation, first the propagation in an aluminium single plate was tested. For that purpose, the theoretical phase velocity extracted from Figure 3 for 500 kHz was used in the Eq. (9). The resulting incident angle for S0 mode, which is the same as the receiving angle, is 18.2°.

The signal collected at the receiver is presented in Figure 9. It is observed an increase in the pulse length, due to the dispersion behavior of the S0 mode phase velocity, when compared with the original three cycle excitation burst (Figure 8 (a)). Besides the direct signal propagated between the transmitter and the receiver, it is also observed an interference signal corresponding to the round trip in the water path at the emitter. To avoid that interference, the distance between the emitter

transducer and the plate should be increased, however such was not possible in the present simulation by limited computational resources. Nevertheless, this fact has not prevented the peak-to-peak amplitude value from being correctly evaluated.

To confirm that the excited propagation mode is indeed S₀, the phase velocity c_p was calculated through the phase spectrum approach [56], as

$$c_p = \frac{2\pi fL}{\Delta\varphi}. \quad (9)$$

where f is the frequency, L is the path difference between two collected signals, and $\Delta\varphi$ is the respective difference in the phase spectrum. Figure 10 illustrates the phase velocity obtained by this method for $L=20\text{mm}$. There is a clear agreement between the presented phase velocity in Figure 10 and the theoretical one shown in Figure 3.

Comparing the peak-to-peak amplitudes of the two above mentioned signals, the attenuation was also computed, resulting in 27.5 Np/m . Again, this value is in full agreement with the theoretical one shown in Figure 4.

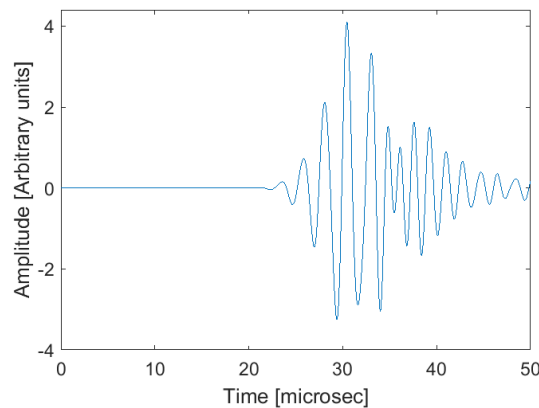


Figure 9. Received signal after propagation in the bonded plate.

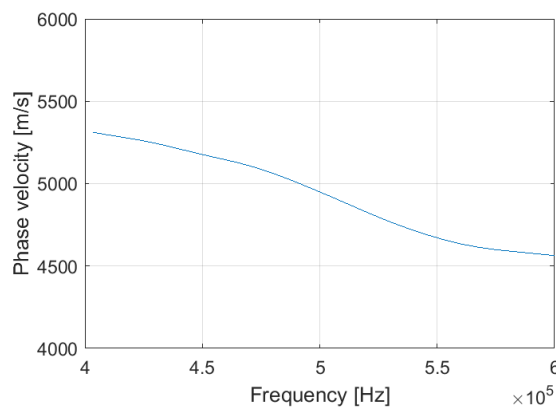


Figure 10. Phase velocity obtained according with Eq. (11).

The same methodology was used to simulate the propagation of S₀ mode in the aluminium bonded plates presented in the Figure 1.

Figure 11 illustrates snapshots of the normal and shear stresses in the XZ plane during the simulation. The emitter transducer is represented by a dashed line on the left. It is clear the high stress values inside the plates. It is also evident the energy leakage surrounding the plates and the absence of shear stress in the water.

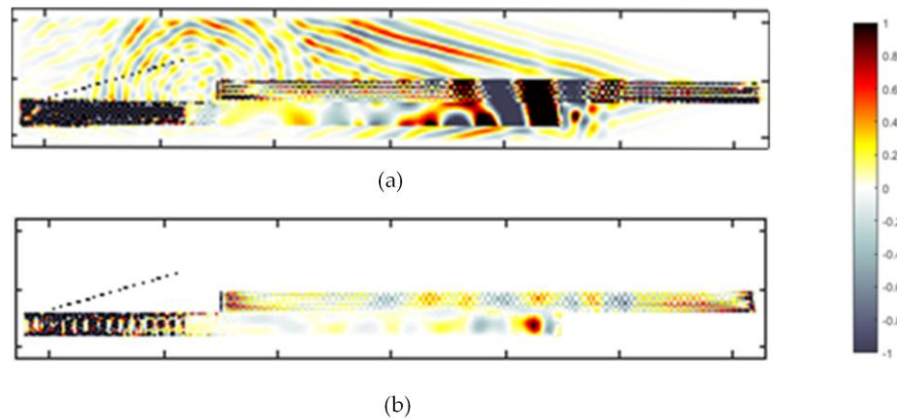


Figure 11. Snapshots of normal (a) and shear (b) stresses in aluminium bonded plates.

The received signal amplitudes corresponding to the propagation in a single plate and in the bonded plates obtained using the same test conditions, were compared. An amplitude decrease of about 10% was observed for the bonded plates compared with the single plate one, which can be justified by the higher attenuation values in the bonded region, when compared to the attenuation of S0 mode in a single plate. This high attenuation is related to the behavior of the existing modes in the bonded zone as result of mode conversion when the wave in the transmitter plate converts to one or more modes at the location where it first meets the adhesive layer. Those modes, which then travel in the bonded region are the natural modes (A0, S0, A1 and S1) of the three-layer system aluminium/adhesive/aluminium. Theoretically, it is expected that to excite a specific mode in the bonded zone, the mode shape in the bottom plate of the bonded zone should be similar to the mode shape in the single transmitter plate [13,59]. Comparing S0 displacement in the single plate (Figure 5 (a)) with the natural modes in bonded plates (Figure 7), it can be said that A1 and S1 modes has completely different shapes, so their amplitude should be very low. The same comparison was made with A0 and S0 mode shapes. Now, despite not being perfectly equal, they have great similarities with S0 in the transmitter plate, which allows saying that these are the dominant modes in the bonded zone. As the mode shape in the bottom plate of the bonded zone is more or less the same for A0 and S0, it can be admitted the same conversion degree for both modes, and using data of Table 2 the average attenuation is 30 Np/m. This value is higher than the one for the single plate, which justify the smaller amplitude measured in the bonded plates.

To evaluate the presence of voids and its influence in the received signal, round air defects (bubbles) with different diameters were simulated, characterizing the absence of the adhesive component between the plates. Figure 12 presents the peak-to-peak amplitude of the receiving signal as a function of void dimensions, normalized with respect to the small void considered (3mm). There is a signal amplitude increase with the void dimensions. The justification for this behavior can be explained because in the presence of a defect, the dominant modes that exist in the bonded joint give rise to additional modes (by mode conversion) that propagates around the defect. In this case this zone could be considered as two isolated semi-immersed plates (at one side there is water and at the other side there is air) where only A0 and S0 mode are allowed to propagate. Figure 13 describes schematically this situation. So, the propagation in the defective bonded joint this zone is similar to the observed in a single plate, and two phenomena contribute to the increase of amplitudes as the defect size increase: (a) as shown previously, the attenuation in the single plate is lower than in the bonded plates, (b) and as one side of the plate is in contact with air, the leakage is half of the verified when the plate is immersed. The experimental results are also presented in the Figure 12. Qualitatively there is reasonable agreement between the simulated and experimental. The observed deviation can be due to the different characteristics of the experimental and simulated defects, which inevitably do not have the same scattering effects.

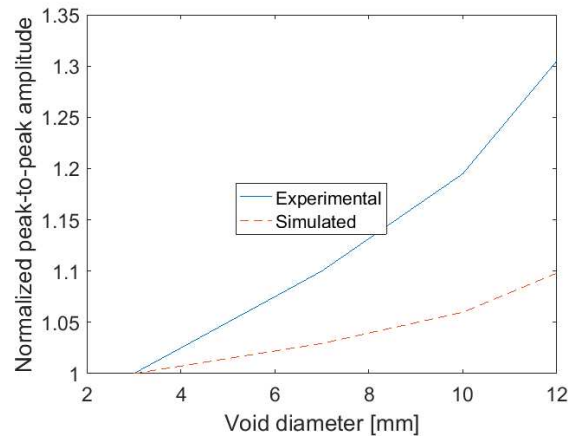


Figure 12. Normalized peak-to-peak amplitude of received signal versus defect diameter.

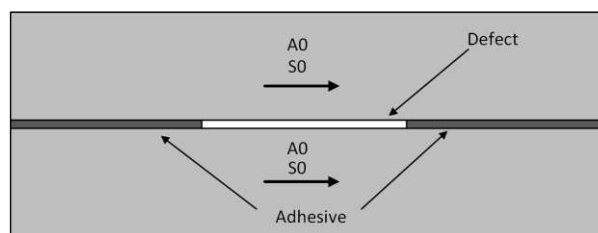


Figure 13. Schematic diagram of existing modes in the overlap region in the presence of a defect.

4. Discussion

In this work the authors present an analytical, simulated, and experimental study about the behavior of ultrasound guided waves propagating in a single plate and in two plates of aluminium, bonded by an epoxy adhesive layer. Both configurations were immersed in water.

For a single plate, a classical iterative optimization algorithm was used to solve the complex dispersion equations in order to obtain the phase velocity, the leakage attenuation and the displacement curves of each propagation mode. It was verified that the high out-of-plane displacement values in the plate surfaces give rise to high attenuation values. For the bonded plates the transfer matrix method was used to obtain the same parameters above. Similar correlations between attenuation and out-of-plane displacements were obtained, as the ones for the single plates. A 3D simulation using the k-Wave MATLAB toolbox was implemented and the results proved its effectiveness to characterize the propagation of guided waves in single and bonded structures, concerning to the correct excitation of a certain mode, and the phase velocity and attenuation measurements. Simulated and experimental air voids with different dimensions were produced in the adhesive region of the bonded joint. An increase in the amplitude of the received signal was observed as the defect size also increased for both simulated and experimental approaches. That behavior is justified by the fact the defective region can be considered as a single plate with lower attenuation, in terms of guided waves propagation. Also, as only one plate surface is in contact with water (the other one is in contact with air), the leakage to water is smaller. The experimental results are in qualitative agreement with the simulated ones. The deviation is related to the inevitable impossibility to reproduce the same defects exactly in simulation and experimental.

Author Contributions: Conceptualization, M.S. and J.S.; methodology, M.S. and J.S.; software, M.S.; validation, M.S. and J.S.; formal analysis, M.S. and J.S.; investigation, M.S. and J.S.; writing—original draft preparation, M.S.; writing—review and editing, M.S. and J.S. All authors have read and agreed to the published version of the manuscript.

Acknowledgments: This research is sponsored by national funds through FCT – Fundação para a Ciência e a Tecnologia, under the project UIDB/00285/2020 and LA/P/0112/2020.

Conflicts of Interest: The authors declare no conflict of interest.

References

1. Adams, R. D.; Drinkwater, B. W. Nondestructive testing of adhesively-bonded joints. *NDT&E* **1997**, *30*, 93–98. DOI: doi.org/10.1016/S0963-8695(96)00050-3.
2. Allin, J.M.; Cawley P.; Lowe M.J. Adhesive disbond detection of automotive components using first mode ultrasonic resonance. *NDT&E* **2003**; *36*, 503–14. DOI: 10.1016/S0963-8695(03)00045-8.
3. Mansfield, T.L. Lamb wave inspection of aluminium sheet. *Mater Eval* **1975**; *33*, 96–100.
4. Ball, D.F.; Shewring D. Some problems in the use of Lamb waves for the inspection of cold-rolled steel sheet coil. *Nondestruct Test* **1976**, *39*(3), 138–45. DOI: doi.org/10.1016/0029-1021(73)90015-7.
5. Alleyne, D.N.; Cawley P. Optimization of Lamb wave inspection techniques. *NDT&E* **1992**, *25*(1), 11–22. DOI: doi.org/10.1016/0963-8695(92)90003-Y.
6. Alleyne, D.N.; Cawley P. The interaction of Lamb waves with defects. *IEEE Trans Ultrason Ferroelectr Freq Control* **1992**, *39*(3), 381–97. DOI: 10.1109/58.143172.
7. Thompson, R.; Alers G.; Tennison M. Application of direct electromagnetic Lamb wave in generation to gas pipeline inspection. In: IEEE Ultrasonic symposium proceedings, NY, USA, 1972. DOI: 10.1109/ULTSYM.1972.196035.
8. Rose, J.L.; Jiao, D.; Spanner J. Ultrasonic guided wave NDT for piping. *Mater Eval* **1996**, *54*(11), 1310–13.
9. Quarry, M.; Rose, J.L. Multimode guided wave inspection of piping using comb transducers. *Mater Eval* **1999**, *57*(10), 1089–90.
10. Jung, Y.; Kundu T.; Ehsani, M. Internal discontinuity detection in concrete by Lamb waves. *Mater Eval* **2001**, *59*(3), 418–23.
11. Rokhlin, S.; Lamb wave interaction with lap-shear adhesive joints: theory and experiment. *J Acoust Soc Am* **1991**, *89*, 2758–65. DOI: doi.org/10.1121/1.400715
12. Rose, J.L.; Rajana, K.M.; Hansch, M.K.T. Ultrasonic guided waves for NDE of adhesively bonded structures. *J Adhes* **1995**, *50*, 71–82. DOI: doi.org/10.1080/00218469508027114.
13. Lowe, M.J.S.; Challis, R.E.; Chan, C.W. The transmission of Lamb waves across adhesively bonded lap joints. *J Acoust Soc Am* **2000**, *107*, 1333–45. DOI: doi.org/10.1121/1.428420.
14. Di Scalea, F.L.; Bonomo, M.; Tuzzeo, D. Ultrasonic guided wave inspection of bonded lap joints: noncontact method and photoelastic visualization. *J Res Nondestruct Eval* **2001**, *13*, 153–71. DOI: doi.org/10.1007/s00164-001-0016-8.
15. Rokhlin, S.I.; Xie, B.; Baltazar, A. Quantitative ultrasonic characterization of environmental degradation of adhesive bonds. *J Adhes Sci Technol* **2004**, *18*, 3, 327–359. DOI: 10.1163/156856104773635463.
16. Baiyang, R.C.; Lissenden J. Ultrasonic guided wave inspection of adhesive bonds between composite laminates, *International Journal of Adhesion and Adhesives* **2013**, *45*, 59-68. DOI: https://doi.org/10.1016/j.ijadhadh.2013.04.001.
17. Matt, H.; Bartoli, I.; Di Scalea, F.L. Ultrasonic guided wave monitoring of composite wing skin-to-spar bonded joints in aerospace structures. *J Acoust Soc Am* **2005**, *118*, 2240-2252. DOI: doi.org/10.1121/1.2033574.
18. Gauthier, C.; El-Kettani, M.; Galyc, J.; Predoi, M.; Leduc, D.; Izbicki, J. Lamb waves characterization of adhesion levels in aluminum/epoxy bi-layers with different cohesive and adhesive properties. *International Journal of Adhesion and Adhesives* **2017**, *74*, 15-20. DOI: doi.org/10.1016/j.ijadhadh.2016.12.002.
19. Yilmaz, B.; Asokkumar, A.; Jasiunien, E.; Kažys, R. Air-Coupled, Contact, and Immersion Ultrasonic Non-Destructive Testing: Comparison for Bonding Quality Evaluation. *Appl Sci* **2020**, *10*, 6757. DOI: 10.3390/app10196757.
20. Mori, N.; Wakabayashi, D.; Hayashi, T. Tangential bond stiffness evaluation of adhesive lap joints by spectral interference of the low-frequency A0 lamb wave. *International Journal of Adhesion and Adhesives* **2022**, *113*, 103071. DOI: doi.org/10.1016/j.ijadhadh.2021.103071
21. Rucka, M.; Wojtczak, E.; Lachowicz, J. Damage Imaging in Lamb Wave-Based Inspection of Adhesive Joints. *Appl Sci* **2018**, *8*(4), 522. DOI:10.3390/app8040522. DOI: doi.org/10.3390/app8040522.
22. Wojtczak, E.; Rucka, M. Wave Frequency Effects on Damage Imaging in Adhesive Joints Using Lamb Waves and RMS, *Materials* **2019**, *12*(11), 1842. DOI: doi.org/10.3390/ma12111842.
23. Nicassio, F.; Carrino, S.; Scarselli, G. Elastic waves interference for the analysis of disbonds in single lap joints. *Mechanical Systems and Signal Processing* **2019**, *128*, 340-351. DOI: doi.org/10.1016/j.ymsp.2019.04.011.
24. Nicassio, F.; Carrino, S.; Scarselli, G. Non-linear Lamb Waves for Locating Defects in Single-Lap Joints. *Front Built Environ, Sec. Computational Methods in Structural Engineering* **2020**, *6*, 45, 1-10. DOI: 10.3389/fbuil.2020.00045.
25. Wang, K.; Liu, M.; Su, Z.; Guo, S.; Cui, F. Mode-mismatching enhanced disbond detection using material nonlinearity in guided waves at low frequency. *Journal of Sound and Vibration* **2021**, *490*, 115733. DOI: doi.org/10.1016/j.jsv.2020.115733.

26. Carrino, S.; Nicassio, F.; Scarselli, G.; Vitolo, R. Finite difference model of wave motion for structural health monitoring of single lap joints. *International Journal of Solids and Structures* **2019**, *161*, 219-227. DOI: <https://doi.org/10.1016/j.ijsolstr.2018.11.019>.
27. Moria, N.; Kusaka, T. Reflection and transmission characteristics of Lamb waves at an adhesive lap joint of plates. *J Acoust Soc Am* **2019**, *145* (5), 3075-85. DOI: 10.1121/1.5109098.
28. Liu, N.; Chen, S.; Wong, Z.; Yao, K.; Cui, F. In situ disbond detection in adhesive bonded multi-layer metallic joint using time-of-flight variation of guided wave. *Ultrasonics* **2020**, *102*, 106062, 1-13. DOI: doi.org/10.1016/j.ultras.2020.106062.
29. Pereira, D.; Le Duff, A.; Painchaud-April, G.; Belanger, P. Simulation-Based Inversion for the Characterization of Adhesively Bonded Joints Using Ultrasonic Guided Waves. *IEEE Trans Ultrason Ferroelectr Freq Control* **2022**, *69*, 7, 2400-7. DOI: 10.1109/TUFFC.2022.3175773.
30. Treeby, B.; Cox, B. k-Wave: MATLAB toolbox for the simulation and reconstruction of photoacoustic wavefields. *J Biomed Opt* **2010**, *15*(2), 21314, 1-12. DOI: 10.1117/1.3360308.
31. Treeby, B.; Jaros, J.; Rendell, A.; Cox, B. Modeling nonlinear ultrasound propagation in heterogeneous media with power law absorption using a k-space pseudospectral method. *J Acoust Soc Am* **2012**, *131*, 4324-4336. DOI: <https://doi.org/10.1121/1.4712021>.
32. Wang, K.; Teoh, E.; Jaros, J.; Treeby, B. Modelling nonlinear ultrasound propagation in absorbing media using the k-Wave toolbox: Experimental validation. In Proceedings of the 2012 IEEE International Ultrasonics Symposium, Dresden, Germany, 7-10 October 2012. DOI: 10.1109/ULTSYM.2012.0130. DOI: 10.1109/ULTSYM.2012.0130.
33. Pérez-Liva, M.; Herraiz, J.; Udías, J.; Miller, E.; Cox, B.; Treeby, B. Time domain reconstruction of sound speed and attenuation in ultrasound computed tomography using full wave inversion. *J Acoust Soc Am* **2017**, *141*, 1595-1604. DOI: doi.org/10.1121/1.4976688.
34. Zhao, X.; McGougha, R. Time-domain analysis of power law attenuation in space-fractional wave equations. *J Acoust Soc Am* **2018**, *144*, 467-477. DOI: doi.org/10.1121/1.5047670.
35. Almansourin, H.; Venkatakrishnan, S.; Bouman, C.; Santos-Villalobos, H. Model-Based Iterative Reconstruction for One-Sided Ultrasonic Nondestructive Evaluation. *IEEE Trans Comput Imaging* **2019**, *5*, 150-164. DOI: 10.1109/TCI.2018.2883218.
36. Matsui, K.; Azuma, T.; Fujiwara, K.; Takeuchi, H.; Itani, K.; Wang, J.; Sakuma, I. Improving high-intensity focused ultrasound beam imaging via a backscattering suppression algorithm. *Jpn J Appl Phys* **2017**, *56*, 57301. DOI: 10.7567/JJAP.56.057301.
37. Acquaticci, F.; Guarracino, J.; Gwirc, S.; Lew, S. A polydimethylsiloxane-based axicon lens for focused ultrasonic brain stimulation techniques. *Acoust Sci Technol* **2019**, *40*, 116-126. DOI: doi.org/10.1250/ast.40.116.
38. Cui, W.; Qin, K. Fast 3-D Ultrasonic Imaging Using Time-Domain Synthetic Aperture Focusing Techniques Based on Circular Scan Conversions. *IEEE Trans Comput Imaging* **2018**, *4*, 632-639. DOI: 10.1109/TCI.2018.2870303.
39. Petrella, L.; Perdigão, F.; Caixinha, M.; Santos, M.; Lopes, M.; Gomes, M.; Santos, J. A-scan ultrasound in ophthalmology: A simulation tool. *Med Eng Phys* **2021**, *97*, 18-24. DOI: <https://doi.org/10.1016/j.medengphy.2021.09.005>.
40. Santos, M.; Santos, J.; Petrella, L. Computational simulation of microflaw detection in carbon-fiber-reinforced polymers. *Electronics* **2022**, *11*, 2836. DOI: doi.org/10.3390/electronics11182836.
41. Brill, T.; Klieber, C. Reflection and mode-conversion of ultrasonic leaky Lamb waves at inaccessible discontinuities in layered structures. In Proceedings of the 2016 IEEE International Ultrasonics Symposium, Tours, France, 18-21 September 2016. DOI: 10.1109/ULTSYM.2016.7728587.
42. Klieber, C.; Brill, T. Mapping of ultrasonic Lamb-wave field in elastic layered structures using laser probes. In Proceedings of the 173rd Meeting of Acoustical Society of America and 8th Forum Acusticum, Boston, MA, USA, 25-29 June 2017. DOI: doi.org/10.1121/2.0000603.
43. Viktorov, A. *Rayleigh and Lamb Waves – Physical Theory and Applications*, Plenum, New York, USA, 1967, pp. 117-118.
44. Rose, J. *Ultrasonic Waves in Solid Media*, Cambridge University Press, Cambridge, UK, 1999, pp.113-115. DOI: doi.org/10.1017/CBO9781107273610.
45. Cawley, P.; Alleyne, D. The Use of Lamb Waves for the Long Range Inspection of Large Structures. *Ultrasonics* **1996**, *34*, 287-290. DOI: [doi.org/10.1016/0041-624X\(96\)00024-8](https://doi.org/10.1016/0041-624X(96)00024-8).
46. Carboni, M.; Giannelo, A.; Giglio, M. A Lamb Waves Based Statistical Approach to Structural Health Monitoring of Carbon Fibre Reinforced Polymer Composites. *Ultrasonics* **2015**, *60*, 51-64. DOI: doi.org/10.1016/j.ultras.2015.02.011.

47. Santos, M.; Perdigão, J. Leaky Lamb waves for the detection and sizing of defects in bonded aluminium lap joints. *NDT&E Int* **2005**, *38*, 561–568. DOI: doi.org/10.1016/j.ndteint.2005.02.004.
48. Chimenti, D.; Rokhlin, S. Relationship between leaky Lamb modes and reflection coefficient zeroes for a fluid-coupled elastic layer. *J Acoust Soc Am* **1990**, *88*, 1603–1611. DOI: doi.org/10.1121/1.400319.
49. Bernard, A.; Lowe, M.; Deschamps, M. Guided waves energy velocity in absorbing and non-absorbing plates. *J Acoust Soc Am* **2001**, *110*(1), 186–196. DOI: doi.org/10.1121/1.1375845.
50. Haskell, N. Dispersion of surface waves on multilayered media. *Bull Seismol Soc Am* **1953**, *43*, 17–34. DOI: doi.org/10.1029/SP030p0086.
51. Lowe M. Matrix techniques for modeling ultrasonic waves in multilayered media. *IEEE Trans Ultrason Ferroelectr Freq Control* **1995**, *42*(4), 525–42. DOI: 10.1109/58.393096.
52. Wang, L.; Rokhlin, S. Stable reformulation of transfer matrix method for wave propagation in layered anisotropic media. *Ultrasonics* **2001**, *39*, 6, 413–424. DOI: doi.org/10.1016/S0041-624X(01)00082-8.
53. Lee, C.; Xu, Y. A modified transfer matrix method for prediction of transmission loss of multilayer acoustic materials. *J Sound Vib* **2009**, *326*, 290–301. DOI: doi.org/10.1016/j.jsv.2009.04.037.
54. Rose, J. *Ultrasonic Guided Waves in Solid Media*. Cambridge University Press, Cambridge, UK, 2014, pp. 227–230. DOI: doi.org/10.1017/CBO9781107273610.
55. Armin, H.; Sause, M. Classification of solutions for guided waves in anisotropic composites with large numbers of layers. *J Acoust Soc Am* **2018**, *144*, 3236–56. DOI: //doi.org/10.1121/1.5082299.
56. Santos, M.; Faia, P. Propagation of Ultrasonic Lamb Waves in Aluminium Adhesively Bonded Lap Joints and in Single Plates. *Res Nondestruct Evaluation* **2009**, *20*, 178–191. DOI: doi.org/10.1080/09349840902755867.
57. Krautkramer J.; Krautkramer H., *Ultrasonic Testing of Materials*, Springer-Verlag Berlin Heidelberg GmbH, 1990, pp. 561. DOI: dx.doi.org/10.1007/978-3-662-10680-8
58. Treeby, B.; Wise, E.; Cox, B. Nonstandard Fourier Pseudospectral Time Domain (PSTD) Schemes for Partial Differential Equations. *Commun Comput Phys* **2018**, *24*(3), 623–634. DOI: doi.org/10.48550/arXiv.1709.02962.
59. Auld, B.; Kino, G. Normal mode theory for acoustic waves and its application to the interdigital transducer. *IEEE Trans Electron Devices* **1971**, *18*(10), 898–908. DOI: 10.1109/T-ED.1971.17303.

Disclaimer/Publisher's Note: The statements, opinions and data contained in all publications are solely those of the individual author(s) and contributor(s) and not of MDPI and/or the editor(s). MDPI and/or the editor(s) disclaim responsibility for any injury to people or property resulting from any ideas, methods, instructions or products referred to in the content.